IEEE Open Journal of
Intelligent Transportation
Systems

Received 22 December 2023; revised 14 February 2024; accepted 16 March 2024. Date of publication 27 March 2024; date of current version 12 April 2024.

Digital Object Identifier 10.1109/OJITS.2024.3380569

An Optimal Routing Framework for an Integrated Urban Power–Gas–Traffic Network

MOHAMMAD JADIDBONAB[1] (Graduate Student Member, IEEE), HUSSEIN ABDELTAWAB[2] (Senior Member, IEEE), AND YASSER ABDEL-RADY I. MOHAMED[1] (Fellow, IEEE)

[1]Department of Electrical and Computer Engineering, University of Alberta, Edmonton, AB T6G 2V4, Canada

[2]Engineering Department, Wake Forest University, Winston-Salem, NC 27101, USA

CORRESPONDING AUTHOR: M. JADIDBONAB (e-mail: jadidbon@ualberta.ca)

This work was supported in part by the Canada First Research Excellence Fund as part of the University of Alberta's Future Energy Systems Research Initiative, and in part by Alberta Innovates.

ABSTRACT This paper develops a risk-averse-based framework for optimizing the operation of an integrated power, gas, and traffic (PGT) network with an application to a typical PGT network in downtown Edmonton, the forefront of Canada's transition to electric vehicles and sustainable urban travel options. The developed non-probabilistic framework provides decision-makers with various secure options to avoid worst-case scenarios and promote social and environmental benefits. The integration of different energy systems allows operators to pursue optimal strategies in critical situations, such as facility outages, maintaining the system within a secure operational range without resorting to expensive workarounds. The proposed algorithm and integrated structure can select optimal travel routes to minimize gas-emission effects and locate charging options to reduce electric vehicle users' travel time. It can mitigate challenges posed by distributed generator outages and roadway closures. The numerical results from implementing the framework on different case studies and the solar-based PGT network of Edmonton indicate its feasibility and effectiveness.

INDEX TERMS Traffic network, travel time, origin-destination pair, power-gas network, information gap theory.

NOMENCLATURE

INDICES

t	Index for time intervals, from 1 to T
$j,\ i,\ r$	Index for OD pairs, candidate routes, and roads
b, b_n, b_h	Set of power network buses and power network buses where charging stations and energy hubs are located
l	Set of power network lines
n	Set of natural gas network nodes

PARAMETERS

NT	Uncongested travel time of road r
ST	Shortest route of j's OD pair travel time
D_T	Traffic demand of j's OD pair
ω	Binary variable that equals 1 if the route of OD pair j passes road r is selected and 0 otherwise
x/y	Proportion of EVs/charging station users
z	Traffic capacity of roads
π^E	Conversion ratio of traffic flow to power
E_u	Capacity of each charging unit
∂^E	Number of charging units
ϑ	Correlation coefficient of routes and charging stations
$D_e^{p/q}$	Active/reactive power demands

The review of this article was arranged by Associate Editor Yajie Zou.

P_b^{Min}/P_b^{Max}	Minimum/maximum boundaries of active generation units
Q_b^{Min}/Q_b^{Max}	Minimum/maximum boundaries of reactive generation units\.
V_b^{Min}/V_b^{Max}	Minimum/maximum boundaries of voltage magnitude
$P_l^{Min/max}/Q_l^{Min/Max}$	Minimum/maximum allowed active/reactive power capacities of the power system lines
G_g	Natural gas gross heating value
κ	A binary matrix (equals 1 when there is a facility between nodes n and m of the natural gas network and 0 otherwise.)
D_g	Gas power demand at the gas network.
π_{nm}^c	The compressor constant located between n^{th} and m^{th} nodes of the natural gas network
$rate_{Min/Max}^c$	Minimum/maximum boundaries of gas compressor pressure
$GS_n^{Min/Max}$	Minimum/maximum boundaries of natural gas suppliers
π_{nm}^{Pipe}	Pipeline flow factor of gas network
$\mathrm{Pr}_{Min/Max}$	Minimum/maximum permissible node pressures
η^{Trans}	Transformer efficiency
$\eta_{e/ht}^{CHP}$	Efficiency of electrical/thermal output of the CHP unit
$\eta_{e/g}^{Boiler}$	Efficiency of the electric/gas-powered boiler.
S_{MS}	PV panels' maximum surface
η_{IE}	PV panels' instantaneous efficiency
η_{MPPT}	Efficiency of the power-tracking device
η_{RE}	Reference efficiency of the PV system
τ	Temperature coefficient of the PV system's efficiency
c_{TC}	Cost coefficient of travel time
$a_e,\ b_e,\ c_e$	Coefficients of power generation units' cost function
$a_g,\ b_g,\ c_g$	Coefficients of gas-supplying unit's cost function
ζ_{LS}	Coefficient of the load-shedding penalty cost
$Z^{CO_2/SO_2/NO_x}$	Emission factor of $CO_2/SO_2/NO_x$
ρ	Cost deviation factor of the risk-averse function
OF_F	Expected total cost.

VARIABLES

ET	Extra travel time
$F_{EV/C}$	Traffic flow of EVs/CFVs
$FC_{EV/C}$	Traffic flow of EVs/CFVs through selected routes
$\beta,\ \gamma,\ \alpha$	Dual variables for equations (2)–(6)
F_{ES}	Traffic flow assigned to the electric charging station
P_{CS}	Electrical loads of the charging stations
P_b/Q_b	Active/reactive power injected to the power system
P_{LS}	Amount of curtailed load
P_{PV}	Solar power generator output
$V,\ \delta$	Voltage magnitude and voltage phase of the power network buses
$Y,\ \theta$	Magnitude and phase of the element of admittance matrix
GS_n	Gas injected into the gas network
P_{nm}^c	Gas power consumed by compressor between n^{th} and m^{th} nodes of the natural gas network
P_{nm}^{Pipe}	Gas power passing through pipeline between n^{th} and m^{th} nodes
GF_{nm}^{Pipe}	Gas flow through the pipe between the n^{th} and m^{th} nodes
P_n	Power injected by the gas-supplying units
GF_{nm}^c	Gas flow through the compressor between n^{th} and m^{th} nodes
Pr_n	Gas pressure at n^{th} node
$P_{e/g}^{Boiler}$	Power consumed by the electrical/gas-powered boilers
P_e^{Trans}	Power consumed by the transformers
$P_{e/ht}^{EH}$	Active power/thermal power demand of the energy hubs
Q_e^{EH}	Reactive power demand of the energy hubs
P^{CHP}	Power consumed by the CHP units
R_R	Solar radiation
C_{OP}	Operational cost of the PGT network
C_T	Travel cost of the traffic network
$C_{P/G}$	Operational cost of the power generators/natural gas system.
C_{PC}	Penalty cost of load shedding
C_{GHE}	Gas emission effect of the PGT system

FUNCTIONS

$U(\widetilde{D}_T, \mu)$	IGR algorithms' uncertainty
$\widehat{\mu}(TOC, OF_{RA})$	IGR algorithms' risk-averse function
GE_{gen}	Emission function of the power system
GE_{CHP}	Emission function of the CHP units
GE_{Boiler}	Emission function of the boilers

I. INTRODUCTION

A. MOTIVATION AND LITERATURE REVIEW

RECENTLY, the threat of climate change has prompted the development of environmentally friendly and cost-efficient transportation technologies [1]. In particular, fast charging technologies and increased battery capacity are encouraging the use of electric vehicles (EVs), and EV charging stations connected to the power grid are proliferating. However, since conventional electrical generators remain the primary energy source, separate assessment of the safety and sustainability of modern traffic and energy

systems is unrealistic. As Edmonton, one of the most polluted cities in Canada, develops fast charging stations [2] and multicarrier energy systems [3], evaluating and improving their integration is a priority for power providers, the energy research community, and system decision-makers.

Few comprehensive studies integrate the urban traffic system with multicarrier energy systems or power-traffic (PT) networks with natural gas networks, which can indicate optimal conditions for meeting and adjusting to power demands. Studies typically focus solely on standalone traffic networks [4], [5] or couple power and traffic networks [6], [7], [8]. The authors of [4] focus on a standalone EV-based traffic model that minimizes charging cost, charging time, and travel time. A Dijkstra search and a metaheuristic evolutionary optimization are applied to solve the path planning problem in [5]. In [6], a PT model combining an 18-bus power distribution system with a 13-node traffic network, is evaluated to optimize charging stations' profit. A traffic congestion management method to optimize the operational costs of traffic and power systems is presented in [7]. A short-term operational problem is solved in [8], where (day ahead) flows are optimized for a 20-bus power/12-node traffic model. Therefore, there is a significant lack of comprehensive studies on integrating the urban traffic system with integrated multicarrier energy systems.

The primary rationale for adopting EVs is to reduce and control conventional energy systems' greenhouse gas emissions. The authors of [6] evaluate emission effects; [4] and [9] propose approaches to reduce the undesirable effects of the traffic system. The authors of [10] propose a method to assess CO_2 emission data as an unpredictable and undesirable output. The gas emissions of conventional vehicles and power generation units are modeled in [11]. An input-output analysis is implemented to assess direct gas emissions from fuel consumption in China's industrial transportation sector [12].

All these studies agree that renewable energy systems significantly reduce the undesirable effects of conventional energy systems' greenhouse gas emissions. Investigations of renewable energy-integrated power systems include a wind-integrated, 24-bus power system proposed to minimize scheduling costs [13]; it implements a conditional value, at-risk method to solve the two-stage stochastic optimization problem. The authors of [14] use a model-free optimization technique to propose a solar-integrated energy hub that reduces operational and emission costs while satisfying thermal and electrical demands. In renewable-based, multicarrier energy systems, storage addresses the problem of intermittence [15].

Gas-powered energy generators remain the standard in power systems studies. Most studies model gas fuel as an input in the optimization problem, considering an ideal system that supplies different gas-powered facilities. For example, in [16], natural gas fuels the boiler and combined heat and power (CHP) units but is treated as an input fuel only for the proposed multicarrier energy system. Natural gas is one of the energy carriers in the standalone local energy hub presented in [17]; while it is designed to supply multiple loads, the natural gas network is not considered. Studies conducted in [18] assess the technical and economic improvements to the power system when integrated with a gas system using two-stage, probabilistic scenario-based stochastic optimization.

No study has yet examined the effects of the conventional gas network on the integrated PT network, although natural gas generators and renewable energy resources are the main pillars of integrated traffic and multicarrier energy systems. Their various uncertain parameters and associated risks must be handled. While the storage and energy hub concepts offer operators and decision-makers some flexibility in handling uncertainty, prediction errors in real-world systems exacerbate risks. Combining a mathematics-based, risk-averse method with integrated urban networks concepts will fortify practical systems against unforeseen conditions following real-time events.

Various methodologies have been devised to contend with uncertain parameters and associated risks. The conditional value at risk (CVaR) algorithm has been applied to manage power demands in the context of uncertain solar power generation [19] and wind and solar power generation [20]. In [21], an energy hub is introduced to minimize operational costs in a multicarrier energy system. Scenario-based stochastic optimization addresses uncertainties linked to wind speed and power demands, while information gap decision theory is employed to manage uncertain energy prices. Another study [22] presents a stochastic method for controlling wind and demand uncertainties. Additionally, it introduces a robust model for managing uncertain prices in a wind-based energy hub system. However, stochastic optimization carries significant computational burdens in modeling realistic large-scale systems, and robust algorithms often assume fixed uncertainties, when, by nature, they change. The information gap-based risk-averse (IGR) strategy can adjust expectations based on forecast values to better model practical integrated power, gas, and traffic (PGT) networks.

In the domain of power systems, numerous studies have delved into uncertainties related to price, load, and renewable resources. One neglected research area concerns the impacts of uncertain traffic flow on integrated power and gas networks. The prevalence of electrical-based urban transportation systems challenges integrated PGT infrastructures. The studies noted above overlook how integrating equipment-based improvements with mathematical risk-management methods could improve decision-making under uncertain, potentially undesirable parameters. The need for comprehensive research on risk-aware management of uncertain traffic flow demands on integrated PGT systems is urgent. Table 1 presents a taxonomy of proposed models to optimize traffic-based energy systems.

TABLE 1. Detailed comparison of models in the literature with the proposed model.

References	Integrated systems			Uncertainty	Risk control	Gas emission reduction
	Traffic network	Power network	Natural gas network			
[4]	✓	✗	✗	✗	✗	✗
[5]	✓	✗	✗	Traffic demand	✗	✗
[6]	✓	✓	✗	✗	✗	✗
[7]	✓	✓	✗	✗	✗	✗
[8]	✓	✓	✗	✗	✗	✗
[9]	✓	✗	✗	✗	✗	✓
[10]	✓	✓	✗	✗	✗	✓
[11]	✓	✓	✗	✗	✗	✓
[20]	✗	✓	✓	Renewable resource	CVaR	✗
Proposed	✓	✓	✓	Traffic demand	Info. Gap-based Risk-Averse	✓

B. CONTRIBUTIONS

The power network's main challenge is securely meeting load requirements. An integrated natural gas network in the PGT system can provide support in critical situations, especially with the increasing penetration of EVs and fast charging stations, which directly reduce greenhouse gas emissions. To the best of our knowledge, this paper presents the first comprehensive approach to optimize traffic patterns and reduce greenhouse gas emissions from conventional fuel-powered facilities in hybrid transportation and multicarrier energy networks (see Table 1). The case study of the downtown Edmonton traffic network provides practical proof of concept, and the model's effectiveness is assessed under various unfavorable circumstances, including distributed generator trip contingencies and road closures. The proposed information gap-based PGT approach promises to achieve optimal power flow and reduce the flow costs of modern traffic networks.

More specifically, the main contributions of this work can be summarized as follows:

- Integrating the natural gas network with the power-traffic network to provide optimal, secure operational conditions while minimizing urban travel costs.
- The proposed PGT system ensures safe and secure operational conditions in the face of adverse events like distributed generator outages and road closures.
- The implemented information gap theory-based risk-averse strategy effectively addresses risks associated with uncertain parameters like traffic demand and guarantees optimal total cost in critical conditions.
- Introducing a novel model for the integration of power, gas, and traffic networks, wherein road congestion is alleviated through the proposed concept.
- Evaluation and reduction of the proposed systems' greenhouse gas emissions.

C. PAPER ORGANIZATION

The remainder of the paper is organized as follows: Section II describes the mathematical model and the technical and economic constraints of the proposed integrated PGT system. Section III demonstrates the IGR optimization method. Section IV discusses the assumptions, case studies, and numerical results of the proposed model. Finally, Section V highlights the conclusions.

II. BACKGROUND

This section explains the mathematical model of the initial deterministic optimization problem based on the predicted parameters. The subsections present a detailed description of the PGT network, technical and economic constraints, and objective function.

A. TRAFFIC NETWORK

The main concept of the proposed traffic network, known as the *origin-destination (OD) pairs traffic model*, posits that each vehicle travels from an origin to a destination; each OD pair has several candidate routes, and each route includes multiple roads. Two approaches can be used to model traffic networks. In the first, the *user equilibrium concept*, users can select the route that takes the least time. In the second, or the *social optimum concept* (discussed in [23]), a central decision-maker arranges the user's plan to minimize total travel time. These concepts are also known as the first and second Wardrop principles. The proposed traffic model also considers both conventional fuel-powered vehicles (CFVs) and EVs.

The second Wardrop-based traffic model can be formulated as in (1)–(7):

$$ET(t) = \sum_{t=1}^{T} \left\{ \sum_{r=1}^{R} NT(r)(F_{EV}(t,r) + F_C(t,r)) - \sum_{j=1}^{J} (ST(j)D_T(t,j)) \right\} \quad (1)$$

where t, r, and j represent the indices for time intervals, traffic roads, and OD pairs, respectively. The extra travel time, $ET(t)$, is defined in (1), where the first term shows the actual travel time, and the second term shows the minimum travel time. Uncongested travel time on road r is denoted as NT, EV traffic flow as F_{EV}, and CFV traffic flow as F_C. The shortest route for j's OD pair travel time is represented by ST, and the traffic demand of j's OD pair by D_T.

The traffic demand of each OD pair should equal the sum of the candidate routes' traffic flow. This principle and the

traffic flow balance for the roads are presented in (2) and (3) for EVs and (4) and (5) for CFVs.

$$F_{EV}(t,r) - \sum_{i=1}^{I}\sum_{j=1}^{J} \omega_{j,i,r}.FC_{EV}(t,j,i) = 0 \tag{2}$$

$$\sum_{i=1}^{I} FC_{EV}(t,j,i) = xy.D_T(t,j) \tag{3}$$

$$F_C(t,r) - \sum_{i=1}^{I}\sum_{j=1}^{J} \omega_{j,i,r}.FC_C(t,j,i) = 0 \tag{4}$$

$$\sum_{i=1}^{I} FC_C(t,j,i) = (1-xy)D_T(t,j) \tag{5}$$

Equations (2) and (3) present the EV traffic flow balance of roads and OD pairs, respectively, while (4) and (5) show the balances for CFVs. Indices for candidate routes are indicated by i, and the traffic flow of EVs or CFVs through selected routes is denoted by $FC_{EV/C}$. The proportion of EVs is represented by x, and the proportion of charging station users by y. Note that ω is a binary variable that equals 1 if the route by which OD pair j passes road r is selected, and 0 otherwise.

The constraints related to road capacity and the principle of positive traffic flow are given in (6) and (7), respectively.

$$F_{EV}(t,r) + F_C(t,r) \le z \tag{6}$$

$$FC_{EV}(t,j,i), FC_C(t,j,i) \ge 0 \tag{7}$$

where z defines the traffic capacity. The proposed model can be reformulated based on the delay that drivers on congested roads experience, defined by a dual variable related to the constraint of the road's capacity. The second Wardrop model assumes no congestion, so it is infeasible for OD path demands, which are higher than road capacities.

The first Wardrop principle, applied in this paper, is closer to the real world. In the proposed traffic network model, the constraints of the initial problem should be satisfied (8). Equations (9)–(12) represent dual constraints associated with the initial traffic model described in (1)–(7). The variables β, γ, and α serve as dual variables for equations (2)–(6). The strong duality theory is illustrated in (13), which indicates that the initial problem is equal to the dual problem. As mentioned, α, which defines the delay on congested roads, indicates a dual variable related to the roads' capacity, presented in (6). In addition, $\beta_{EV/CFV}$, and $\gamma_{EV/CFV}$ denote the dual variables of the initial traffic model given in (2)–(7).

$$Eqs.\ (2)-(7) \tag{8}$$

$$\beta_{EV}(t,r) - \alpha(t,r) = NT(r) \tag{9}$$

$$\gamma_{EV}(t,j) - \sum_{r=1}^{R} \omega_{j,i,r}\beta_{EV}(t,r) \le 0 \tag{10}$$

$$\beta_C(t,r) - \alpha(t,r) = NT(r) \tag{11}$$

$$\gamma_C(t,j) - \sum_{r=1}^{R} \omega_{j,i,r}\beta_C(t,r) \le 0 \tag{12}$$

$$\begin{aligned} xy\sum_{t=1}^{T}\sum_{j=1}^{J}(\gamma_{EV}(t,j)D_T(t,j)) \\ +(1-xy)\sum_{t=1}^{T}\sum_{j=1}^{J}(\gamma_C(t,j)D_T(t,j)) - \sum_{t=1}^{T}\sum_{r=1}^{R}(z.\alpha(t,r)) \\ = \sum_{t=1}^{T}\sum_{j=1}^{J}(ST(j)D_T(t,j)) \\ +\sum_{t=1}^{T}\sum_{r=1}^{R} NT(r)(F_{EV}(t,r)+F_C(t,r)) \end{aligned} \tag{13}$$

$$\alpha(t,r) \ge 0 \tag{14}$$

The proposed traffic network is connected to the power network by electric charging stations. Their capacity and the relationships between the traffic flow assigned to them and their available loads are indicated in (15) and (16).

$$\pi^E.F_{ES}(t,b_n) = P_{CS}(t,b) \tag{15}$$

$$P_{CS}(t,b_n) \le E_u \times \partial^E \tag{16}$$

where F^{ES} and P^{ES} show the traffic flow assigned to the station and the station's demands. The conversion ratio of traffic flow to power is denoted by π^E, the capacity of each charging unit is represented by E_u, and the number of units is indicated by ∂^E.

Constraint (17) guarantees that the charging flow allocated to each station remains below or equal to the total sum of charging flows for all routes passing through these charging stations. Charging flow balance is introduced in (18). Note that ϑ is the correlation coefficient of routes and charging stations. If an OD pair route passes a charging station, the value is 1, and 0 otherwise.

$$F_{ES}(t,b_n) \le \sum_{i=1}^{I}\sum_{j=1}^{J}\left(\vartheta^E_{t,j,i}.FC_{EV}(t,j,i)\right) \tag{17}$$

$$\sum_{n=1}^{N} F_{ES}(t,b_n) = x.\sum_{j=1}^{J} D_T(t,j) \tag{18}$$

B. POWER NETWORK

This section provides the AC power flow method and mathematical models of the power network.

1) AC POWER FLOW MODEL

Active and reactive power balances are satisfied and formulated based on equations (19) and (20), respectively.

$$\begin{aligned} P_b(t) = D^p_e(t,b) + P_{CS}(t,b) - P_{LS}(t,b) - P_{PV}(t,b) \\ +\sum_{c=1}^{B} V(t,b)V(t,c)Y_{bc}\cos(\delta_b - \delta_c - \theta_{bc}), \\ \forall b = 1,\ldots,B \end{aligned} \tag{19}$$

$$Q_b(t) = D_e^q(t,b) + \sum_{c=1}^{B} V(t,b)V(t,c)Y_{bc}\sin(\delta_b - \delta_c - \theta_{bc}), \quad \forall b = 1,\ldots,B \tag{20}$$

where b represents the set of power network buses. Active/reactive power demands are given by $D_e^{p/q}$, and demands of the charging stations/load shedding/solar power generation are defined by $P_{CS/LS/PV}$. V stands for bus voltage magnitude, δ for bus voltage phase, Y for admittance matrix magnitude, and θ for admittance matrix phase.

2) RANGES OF ACTIVE AND REACTIVE POWER

The capacities of the active and reactive generation units are limited by:

$$P_b^{Min} \le P_b(t) \le P_b^{Max}, \ \forall b = 1,\ldots,B \tag{21}$$
$$Q_b^{Min} \le Q_b(t) \le Q_b^{Max}, \ \forall b = 1,\ldots,B \tag{22}$$

3) VOLTAGE CONSTRAINTS

The voltages of the power system buses must be kept in the permissible range. This constraint is described by (23).

$$V_b^{Min} \le V_b(t) \le V_b^{Max}, \ \forall b = 1,\ldots,B_{PQ} \tag{23}$$

4) RANGE OF THE POWER SYSTEM'S LINES

Power system lines must be operated at the allowed capacities. This limitation is applied by (24) and (25):

$$P_l^{Min} \le P_l(t) \le P_l^{Max}, \ \forall l = 1,\ldots,L \tag{24}$$
$$Q_l^{Min} \le Q_l(t) \le Q_l^{Max}, \ \forall l = 1,\ldots,L \tag{25}$$

where the set of power network lines is given by L.

C. NATURAL GAS NETWORK

1) NATURAL GAS SYSTEM'S POWER BALANCE

The power balance of the gas network nodes is given in (26). Equations (27) and (28) model the power flow, or the gas flow multiplied by the gross heating value.

$$GS_n(t) \times G_g = D_g(t,n) + \sum_{m=1}^{M}\left(\kappa_{nm}^c P_{nm}^c(t)\right) + \sum_{m=1}^{M}\left(\kappa_{nm}^{Pipe} P_{nm}^{Pipe}(t)\right) \tag{26}$$
$$P_{nm}^{Pipe}(t) = GF_{nm}^{Pipe}(t) \times G_g \tag{27}$$
$$P_n(t) = GS_{n_s}(t) \times G_g \tag{28}$$

where the gross heating value is represented by G_g, injected gas by GS, and gas power demand at the gas network node by D_g. P^c indicates compressor gas power demand, and gas power transferred from the n^{th} to the m^{th} node is denoted by P_{nm}^{Pipe}. GF_{nm}^{Pipe} shows gas flow through the pipe between the n^{th} and m^{th} nodes. The net power in the n^{th} node should be zero based on the gas network's power balance. In other words, the net power is the sum of consumed, exported, and imported gas power. κ is introduced as a binary matrix with any element equal to 1 when there is a facility between nodes n and m, and 0 otherwise. The proof of equations related to the power flow of natural gas systems can be found in [24].

2) COMPRESSOR MODEL

The compressor keeps the pressure of the natural gas system's nodes in a convenient range. Its gas power flow is calculated based on (29), and the gas consumption of the compressor installed between nodes n and m is presented in (30). Under the following constraints, the compressor constant is defined by π_{nm}^c, and the acceptable pressure range can be formulated as (31).

$$P_{nm}^c(t) = GF_{nm}^c(t) \times G_g \tag{29}$$
$$GF_{nm}^c(t) = \pi_{nm}^c \times GF_{nm}^{Pipe}(t)(\mathrm{Pr}_n(t) - \mathrm{Pr}_m(t)) \tag{30}$$
$$rate_{Min}^c \le \varepsilon(t) \le rate_{Max}^c \tag{31}$$

where $\varepsilon(t) = \frac{\mathrm{Pr}_m(t)}{\mathrm{Pr}_n(t)}$. The gas pressure at the natural gas nodes is defined by Pr.

3) CONSTRAINTS OF THE NATURAL GAS SUPPLIERS

The capacities of the natural gas suppliers are:

$$GS_n^{Min} \le GS_{n_s}(t) \le GS_n^{Max}, \ \forall n_s = 1,\ldots,N_S \tag{32}$$

where N_S represents the set of gas supplier units.

4) GAS FLOW OF THE PIPELINES

The natural gas flow between nodes n and m is given by (33). The pipeline flow factor is shown by π_{nm}^{Pipe}. This value is defined based on the ignorable impacts of gas temperature on its flow through the pipeline [25], [26]. The *sign* function equals 1 if the pressure at the n^{th} node is greater than that at the m^{th} node, and the function equals -1 otherwise.

The permissible node pressures of the gas network are demonstrated in (34), where they have to be kept between Pr_{Min}, and Pr_{Max}.

$$GF_{nm}^{Pipe}(t) = \pi_{nm}^{Pipe}.sign(\mathrm{Pr}_m(t), \mathrm{Pr}_n(t)) \times \sqrt{sign(\mathrm{Pr}_m(t), \mathrm{Pr}_n(t))\left(\mathrm{Pr}_m^2(t) - \mathrm{Pr}_n^2(t)\right)} \tag{33}$$
$$\mathrm{Pr}_{Min} \le \mathrm{Pr}_n(t) \le \mathrm{Pr}_{Max}, \ \forall n = 1,\ldots,N \tag{34}$$

D. ENERGY HUB UNIT

The proposed energy hub concept integrates the power network, gas network, and thermal system. The CHP is its main component. Together, CHP output power and active power imported from the grid meet the energy hubs' load demand. The active load of the h^{th} energy hub, which is located at the b^{th} bus, includes power imported from the energy hub transformer and the electric boiler's consumption. The b_h^{th} bus determines the bus b^{th} from the power network, where the h^{th} energy hub is located. Based on the mentioned assumptions, the active power and heating balances of the energy hub are determined as follows:

$$D_e^P(t,b_h) = P_e^{Boiler}(t,h) + P_e^{Trans}(t,h), b_h \in H, \quad h = 1,\ldots,H \tag{35}$$
$$P_e^{EH}(t,h) = \eta_e^{CHP}P^{CHP}(t,h) + \eta^{Trans}P_e^{Trans}(t,h), \quad h = 1,\ldots,H \tag{36}$$

$$Q_e^{EH}(t,h) = \frac{P_e^{EH}(t,h)}{\eta^{Trans}}, \quad h = 1,\ldots,h \tag{37}$$

$$D_{ht}^{G}(t,h) = P_g^{Boiler}(t,h) + P^{CHP}(t,h), h = 1,\ldots,H \tag{38}$$

$$P_{ht}^{EH}(t,h) \le \eta_{ht}^{CHP} P^{CHP}(t,h) + \eta_e^{Boiler} P_e^{Boiler}(t,h) + \eta_g^{Boiler} P_g^{Boiler}(t,h), \quad h = 1,\ldots,H \tag{39}$$

where η^{Trans} and $\eta_{e/ht}^{CHP}$ describe the efficiencies of the transformer and electrical/thermal output of the CHP, respectively.

E. SOLAR POWER GENERATION SYSTEM

Photovoltaic power generation depends on various metrological variables, such as irradiance, temperature, and geographical location. Equation (40) provides the power generated from solar radiation. The main data on environmental temperature and solar radiation are taken from the meteorological sites of GeoModel Solar [27].

$$P_{PV}(t,b) = S_{MS}.\eta_{IE}.R_R(t,b) \tag{40}$$

P_{PV} refers to solar radiation, S_{MS} to the panels' maximum surface, and η_{IE} to the PV panels' instantaneous efficiency. System efficiency is formulated as:

$$\eta_{IE} = \eta_{MPPT}.\eta_{RE}.[1 - \tau(T_P - T_{RP})] \tag{41}$$

The reference temperature and power-tracking efficiency of the solar panels are assumed to be $25°C$ and 1, respectively. The panels' temperature coefficient can vary from 0.004 to 0.006 per $1°C$. Here, it is assumed to be 0.0048. Panel temperature has an undeniable effect on performance (see [28] for more detail on calculating panel temperature and total solar radiation).

F. OBJECTIVE FUNCTION

To include the operational cost and gas emission effect, the objective function includes two terms, formulated in (42) and (43):

$$Total\ operation\ Cost = \sum_{t=1}^{T} C_{OP}(t) \tag{42}$$

$$Gas\ Emission = \sum_{t=1}^{T} C_{GHE}(t) \tag{43}$$

Equation (44) presents the operational cost of the PGT system. The first and second terms, C_T and C_P, indicate the travel cost of the traffic network and the operational cost of the distributed generators of the power network, respectively. A third term, C_G, shows the operational cost of the natural gas system, and the fourth, C_{PC}, represents the load-shedding cost.

$$C_{OP}(t) = C_T(t) + C_P(t) + C_G(t) + C_{PC}(t) \tag{44}$$

$$C_T(t) = c_{TC}\left\{\sum_{r=1}^{R}[(F_{EV}(t,r) + F_C(t,r))(NT(r) + \alpha(t,r))] - \sum_{j=1}^{J}(PT(j)D_T(j))\right\} \tag{45}$$

$$C_P(t) = \sum_{b=1}^{B} a_e P_b^2(t) + b_e P_b(t) + c_e \tag{46}$$

$$C_G(t) = \sum_{n=1}^{N} a_g P_n^2(t) + b_g P_n(t) + c_g \tag{47}$$

$$C_{PC}(t) = \zeta \sum_{b=1}^{B} P_{LS}(t,b) \tag{48}$$

where the cost coefficient of the travel time is given by C_{TC}, and ζ represents the coefficient of the load-shedding penalty cost.

The emission functions of the power system, CHP units, and boilers are given in (49)–(52).

$$C_{GHE}(t) = \zeta_{ec}\left(GE_{gen}(t) + GE_{CHP}(t) + GE_{Boiler}(t)\right) \tag{49}$$

$$GE_{gen}(t) = \sum_{b=1}^{B} P_b(t) \times \left(z_{gen}^{CO_2} + z_{gen}^{SO_2} + z_{gen}^{NO_x}\right) \tag{50}$$

$$GE_{CHP}(t) = \sum_{b=1}^{B} P_{CHP}(t,b) \times \left(z_{CHP}^{CO_2} + z_{CHP}^{SO_2} + z_{CHP}^{NO_x}\right) \tag{51}$$

$$GE_{Boiler}(t) = \sum_{h=1}^{H} P_{Boiler}(t,h) \times \left(z_{Boiler}^{CO_2} + z_{Boiler}^{SO_2} + z_{Boiler}^{NO_x}\right) \tag{52}$$

where CO_2, SO_2, and NO_x emission factors are represented by Z^{CO_2}, Z^{SO_2}, and Z^{NO_x}, respectively. The emission cost factor is defined by ζ_{ec}.

III. A NEW STRATEGY BASED ON INFORMATION GAP THEORY

The information gap theory is a powerful, non-probabilistic, risk-averse algorithm that can control for uncertain parameters that hamper optimization, giving operators flexible options under real-time conditions. They select the desired targets, and the IGR algorithm maximizes the error horizon between the optimal and forecast uncertainties to guarantee the target [21].

Here, the IGR algorithm is used to reformulate the proposed integrated model, immunizing it to the undesirable effects of uncertain traffic demand. The uncertain model defines the information gap between the forecast and uncertain values of this parameter. Strictly speaking, the algorithm can be implemented as an envelope-bound uncertainty model, where the forecast value defines envelope formation.

The interval of uncertainty can be presented as in (53). Forecasted traffic demand is represented by $\widetilde{D}_T$, uncertain traffic demand is defined by D_T, and the horizon of uncertainty is shown by μ.

$$\forall\mu \in U(\widetilde{D}_T, \mu) = \left\{D_T : |D_T(t,j) - \widetilde{D}_T| \le \mu\widetilde{D}_T\right\}, \ \mu \ge 0 \tag{53}$$

The decision-maker now has the flexibility to immunize the integrated traffic, power, and gas network to the high total costs incurred when traffic demands become critical. In the following optimization problem, OF_{RA}

describes the critical cost of the worst-case uncertain parameters.

$$\widehat{\mu}(TOC, OF_{RA}) = Maximize\left\{\mu : \left[\underset{D_T \in U(\widetilde{D}_T,\mu)}{Maximize}\ OF(TOC, D_T) \leq OF_{RA}\right]\right\} \quad (54)$$

where the portion of the total cost related to traffic demand is defined by TOC. By applying the proposed IGR algorithm, the model's objective function maximizes the uncertain variation while satisfying the technical and economic constraints of the problem. As a result, the predesignated maximum total cost can be guaranteed.

First, the impact of traffic demand on the objective function must be separated from the other terms of the total cost. The objective function can be reformulated as:

$$OF = \sum_{t=1}^{T}\left(OF'(t) + \sum_{j=1}^{J}(D_T(t,j)PT(j))\right) \quad (55)$$

where $OF'(t)$ describes the cost of the proposed system without the contribution of traffic demand.

The proposed bi-level IGR-based optimization problem can be defined as in (56). The lower level focuses on finding the maximum total cost, and based on it, the upper level maximizes the uncertainty horizon. The system's maximum cost is obtained from the maximum value of traffic demand, which equals the maximum value of the interval assumed in (56): $D_T(t,j) = \widetilde{D}_T(1+\mu)$. Therefore, the proposed bi-level problem (56) can be reframed as a single-level optimization problem (57).

$$\begin{cases} \widehat{\mu}(TOC, OF_{RA}) = Maximize\ \mu \\ Subject\ to: \\ Eqs.\ (8) - (52) \\ Maximize \sum_{t=1}^{T}\left(OF'(t) + \sum_{j=1}^{J}(D_T(t,j)PT(j))\right) \leq OF_{RA} \\ OF_{RA} = OF_F(1+\rho) \\ \widetilde{D}_T(1-\mu) \leq D_T(t,j) \leq \widetilde{D}_T(1+\mu) \end{cases} \quad (56)$$

$$\begin{cases} \widehat{\mu}(TOC, OF_{RA}) = Maximize\ \mu \\ Subject\ to: \\ Eqs.\ (8) - (52) \\ \sum_{t=1}^{T}\left(OF'(t) + \sum_{j=1}^{J}(\widetilde{D}_T(1+\mu)PT(j))\right) \leq OF_{RA} \\ OF_{RA} = OF_F(1+\rho) \end{cases} \quad (57)$$

where ρ is the cost-deviation factor, and μ shows the IGR-based problem's objective function. In other words, μ represents an uncertain variable. Figure 1 is a schematic of the proposed algorithm.

The proposed model's decision variables include the generation of electrical and thermal energies by facilities, curtailment of loads, inputs and outputs of the compressors and energy hubs, states of charging stations, traffic flow, and IGR-based deviation factors. The detailed structure of the problem is presented in Fig. 2.

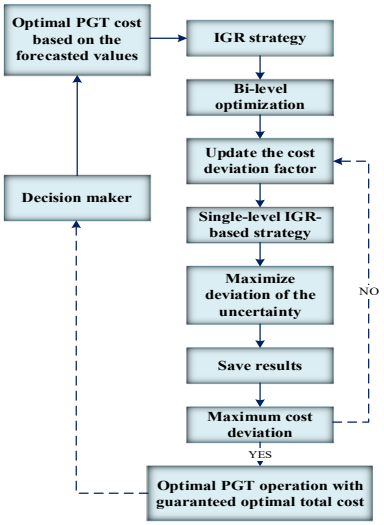

FIGURE 1. Overall schematic of the proposed IGR-based method.

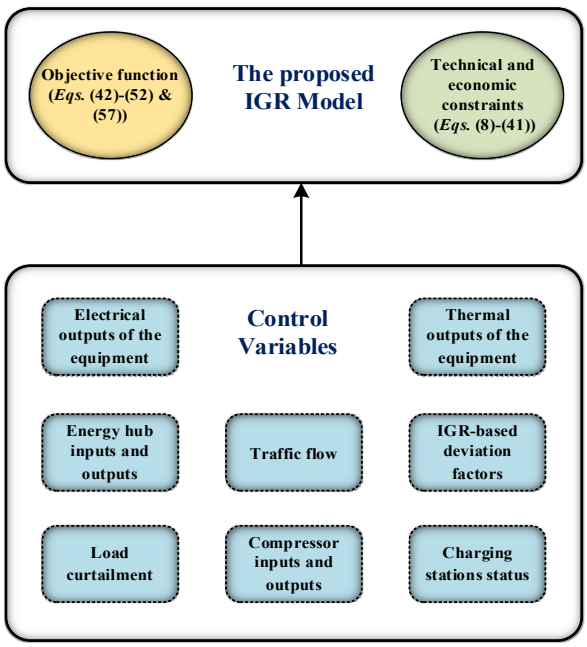

FIGURE 2. Overall structure of the proposed problem.

IV. RESULTS AND DISCUSSION

The proposed method was applied to a system in downtown Edmonton, Canada. The analysis compares the following operational modes, or case studies.

1. A 7-node natural gas network and integrated 14-bus power and 12-node traffic networks;
2. integrated 14-bus power with 7-node natural gas and 12-node traffic (PGT) networks;

TABLE 2. OD pairs' origins and destinations.

OD pair	Origin (traffic network's node)		Destination (traffic network's node)	
	Case #1 and #2	Case #3 and #4	Case #1 and #2	Case #3 and #4
First OD pair	#1	#1	#12	#9
Second OD pair	#7	#14	#6	#4
Third OD pair	#3	#2	#11	#10
Fourth OD pair	#10	#2	#1	#15
Fifth OD pair	#2	-	#7	-
Sixth OD pair	#6	-	#3	-

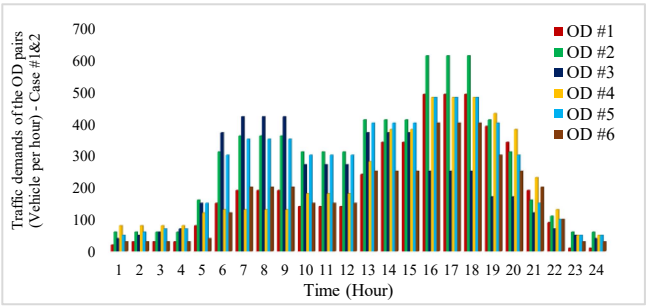

FIGURE 3. Traffic demands of the OD pairs for cases #1 and #2.

3. A 7-node natural gas network and integrated 14-bus power and 18-node traffic networks (Edmonton case study); and
4. integrated 14-bus power with 7-node natural gas and 18-node traffic networks (Edmonton case study, PGT network).

The gas network is separated from the integrated power and traffic (PT) network in the first and third modes. In other words, they follow independent operating policies. The power and gas networks in all four modes are designed based on downtown Edmonton data [29] and structure. The first and second cases represent a well-known, 12-node traffic network. The third and fourth cases mathematically model data for downtown Edmonton, where a CHP unit was recently built [2]. That traffic network, running between 104th Avenue, Rowland Road, 97th Avenue, and River Valley Road, is heavily used on weekdays [30], [31]. It is modeled as an 18-node, 27-road OD pair. Five fast charging stations are located in the area, operated under the Tesla, Flo, and ChargePoint companies [32]. Table 2 shows the origins and destinations of the OD pairs.

The third case study is based on the independently modified 7-node gas network and the integrated 14-bus power and 18-node downtown Edmonton traffic network. The fourth case is the integrated 14-bus power, 7-node natural gas, and 18-node Edmonton PGT network. Figures 3 and 4 illustrate the traffic demands for OD pairs in case studies #1, #2, #3, and #4.

The IGR strategy aims to make the proposed solar-based PGT system immune to undesirable traffic demands. Table 3 indicates the parameters and locations of the energy hub components in the test systems. In the first and third cases, the gas network meets all thermal demands.

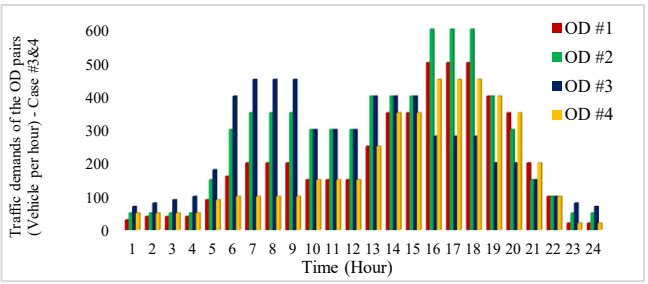

FIGURE 4. Traffic demands of the OD pairs for cases #3 and #4.

TABLE 3. Locations and parameters of the energy hub units.

Energy hub	Elec. bus	Gas node	Efficiencies				
			Thermal CHP	Elec. CHP	Trans.	gas Boiler	Elec boiler
#1	2	7	50	40	100	90	80
#2	13	3	50	40	100	90	80

In the second and fourth case studies, integrated electrical and gas networks satisfy the thermal and electrical demands of the nodes and buses, where energy hubs are located.

The locations and values of the thermal demands are the same in all four case studies. In the PGT network, CHP units and electrical and gas-powered boilers meet the thermal demands of energy hubs. In the first and third cases, gas-powered boilers located in the nodes of the gas network meet thermal demands. Boiler efficiency is 0.9. The values of the emission factors and solar power system can be found in [33] and [28], respectively. The load curtailment penalty cost is assumed to be 150 (cents/kW). Control variables are (a) facility-generated electrical and thermal energies, (b) load curtailment, (c) compressor and energy hub inputs and outputs, (d) charging station states, (e) traffic flow, and (f) IGR-based deviation factors (see Fig. 5 for the detailed structure of the system and charging station locations). The capacity of each fast charging station is 200 kW [34]. Numerical tests were executed by the SBB solver in the GAMS environment with an Intel Core i7-11700k CPU (3.6 GHz) and a 32-GB RAM computer.

A. CASE STUDIES #1 AND #2: TOTAL COST AND POWER CONSUMED AT CHARGING STATIONS

Table 4 shows the emission effects and operation costs of the proposed model. The total cost of Case Study #2 falls from \$5,310.00 to \$5,177.90, or about 2.6% less than in the independent operation. The greenhouse gas emission effect is about 10.6% less, which shows the undeniable influence of the proposed model on environmentally destructive fossil-fuel systems. In the integrated mode, the natural gas system satisfies the power network's electrical demands through the CHP units of the energy hubs, reducing the operational cost of the electrical network from \$3,600.60 to \$3,420.50 in 24 hours. The travel cost of the traffic network is up to

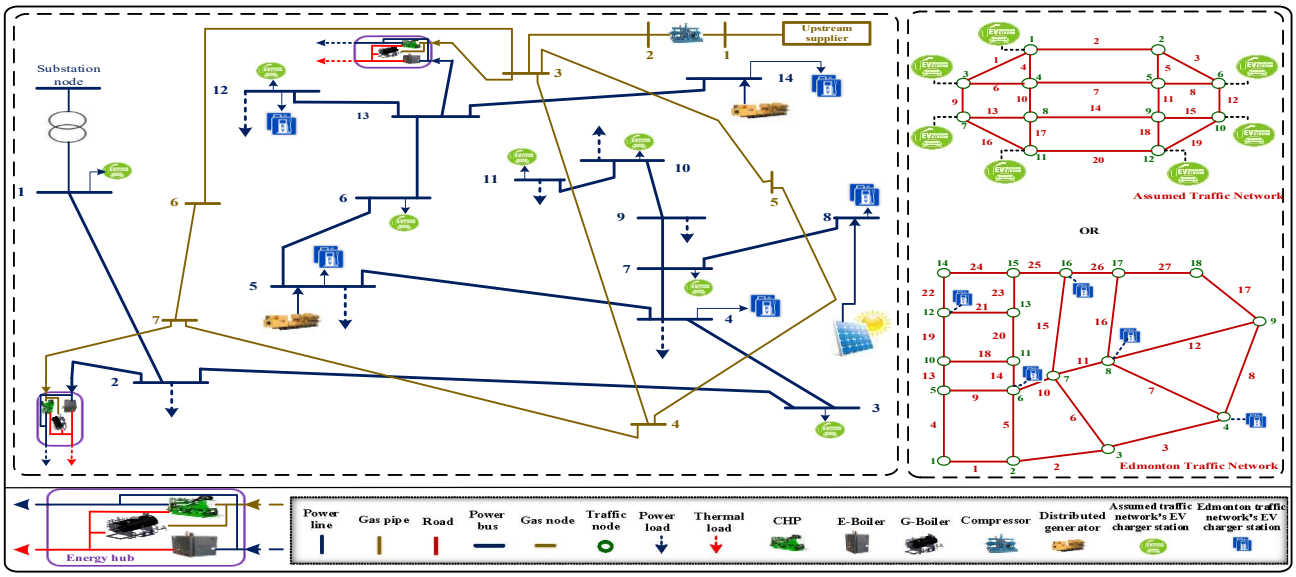

FIGURE 5. Overall structure of the proposed solar-based PGT system.

TABLE 4. Optimal results of case studies #1 and #2.

Case Study	Total cost ($)	Electrical Network cost ($)	Gas Network cost ($)	Travel Cost ($)	Emission (lb)
#1	5310.0	3600.6	1279.8	429.4	3322.8
#2	5177.9	3420.5	1350.4	407.0	2969.2

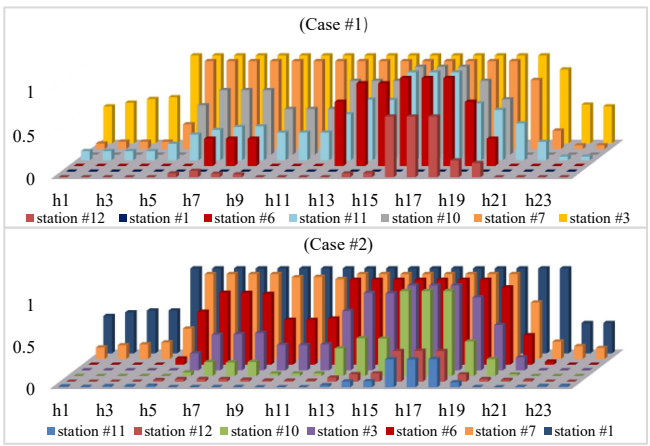

FIGURE 6. Cases 1 and 2: Optimal power charging station consumption (pu).

5.2% less. Lacking load curtailment, the penalty costs in Cases #1 and #2 are zero. Figure 6 shows the power the charging stations consume during the operational horizon. In the independent operation, only the charging stations located on buses 4, 8, and 14 serve EVs from hours 1 to 12, while in the integrated PGT network, EV battery charging is shared among the charging stations on buses 4, 5, 8, 12, and 14, so they operate in a range below their maximum capacity, thus providing a more secure and flexible operating condition, especially during peak hours and critical contingencies.

TABLE 5. Optimal results for case studies #3 and #4.

Case study	Total cost ($)	Electrical network cost ($)	Gas network cost ($)	Travel cost ($)	Emission (lb)
#3	4460.4	2923.8	1279.8	256.7	3020.1
#4	4220.5	2610.3	1375.2	234.9	2559.0

TABLE 6. Case study #3: optimal traffic flows among the OD pairs' candidate routes.

Time (Hour)	Optimal traffic flows (Vehicle per hour)											
	OD #1			OD #2			OD #3			OD #4		
	Candidate routes			Candidate routes			Candidate routes			Candidate routes		
	#1	#2	#3	#1	#2	#3	#1	#2	#3	#1	#2	#3
1	30	0	0	0	0	50	0	70	0	0	0	50
2	40	0	0	0	0	50	0	80	0	0	0	50
3	40	0	0	0	0	50	0	90	0	0	0	50
4	40	0	0	0	0	50	0	100	0	0	0	50
5	90	0	0	0	0	150	0	180	0	0	0	90
6	0	0	160	200	0	100	20	380	0	100	0	0
7	0	0	200	340	0	10	70	380	0	100	0	0
8	0	0	200	340	0	10	70	380	0	100	0	0
9	0	0	200	340	0	10	70	380	0	100	0	0
10	0	0	150	140	0	160	0	300	0	70	0	80
11	0	0	150	140	0	160	0	300	0	70	0	80
12	0	0	150	140	0	160	0	300	0	70	0	80
13	0	0	250	290	0	110	20	380	0	0	0	250
14	0	50	300	330	0	70	20	380	0	0	0	350
15	0	50	300	330	0	70	20	380	0	0	0	350
16	0	250	250	470	0	130	0	280	0	0	0	450
17	0	250	250	470	0	130	0	280	0	0	0	450
18	0	250	250	470	0	130	0	280	0	0	0	450
19	20	0	380	400	0	0	0	200	0	0	0	400
20	0	0	350	300	0	0	0	200	0	30	0	320
21	20	0	170	0	0	150	0	150	0	0	0	200
22	100	0	0	0	0	100	0	100	0	0	0	100
23	20	0	0	0	0	50	0	80	0	0	0	20
24	20	0	0	0	0	50	0	70	0	0	0	20

B. CASE STUDIES #3 AND #4: TOTAL COSTS AND TRAFFIC FLOWS

One of the main goals of the proposed model is to reduce greenhouse gas emissions. Table 5 shows that emissions from the integrated, solar-based PGT network dropped from

TABLE 7. Case study #4: optimal traffic flows among the OD pairs' candidate routes.

Time (Hour)	Optimal traffic flows (Vehicle per hour)											
	OD #1			OD #2			OD #3			OD #4		
	Candidate routes			Candidate routes			Candidate routes			Candidate routes		
	#1	#2	#3	#1	#2	#3	#1	#2	#3	#1	#2	#3
1	30	0	0	50	0	0	0	70	0	0	0	50
2	40	0	0	50	0	0	0	80	0	0	0	50
3	40	0	0	50	0	0	0	90	0	0	0	50
4	40	0	0	50	0	0	0	100	0	0	0	50
5	90	0	0	15	0	0	0	180	0	0	0	90
6	160	0	0	300	0	0	20	380	0	0	0	100
7	130	0	70	350	0	0	70	380	0	0	0	100
8	130	0	70	350	0	0	70	380	0	0	0	100
9	120	0	80	350	0	0	70	380	0	0	0	100
10	130	0	20	300	0	0	0	300	0	0	0	150
11	130	0	20	300	0	0	0	300	0	0	0	150
12	140	0	10	300	0	0	0	300	0	0	0	150
13	0	0	250	380	0	20	20	380	0	0	0	250
14	0	50	300	330	0	70	20	380	0	0	0	350
15	0	50	300	340	0	60	20	380	0	0	0	350
16	0	250	250	470	0	130	0	280	0	0	0	450
17	0	250	250	470	0	130	0	280	0	0	0	450
18	0	250	250	470	0	130	0	280	0	0	0	450
19	0	20	380	400	0	0	0	200	0	0	0	400
20	100	0	250	300	0	0	0	200	0	0	0	350
21	200	0	0	150	0	0	0	150	0	0	0	200
22	100	0	0	100	0	0	0	100	0	0	0	100
23	20	0	0	50	0	0	0	80	0	0	0	20
24	20	0	0	50	0	0	0	70	0	0	0	20

TABLE 8. Operation costs under different contingencies.

Contingency type	Case study	Electrical Network cost ($)	Gas Network cost ($)	Travel Cost ($)	Load shedding cost ($)	Total cost ($)
Road #15 closure	#3	3470.10	1279.8	290.42	0	5040.32
	#4	2998.47	1427.69	262.87	0	4689.03
Distributed generator trip	#3	5220.00	1279.8	544.22	18724.00	25768.02
	#4	3377.54	2996.35	269.35	9817.05	16460.29

TABLE 9. Optimal locations and amounts of load-shedding buses under the distributed generator's trip condition (p.u.).

Electrical bus number #	Case Study #3	Case Study #4
#1	0	0
#2	0.048	0.048
#3	0	0
#4	0.025	0
#5	0.005	0
#6	0	0
#7	0	0
#8	0	0
#9	0	0
#10	0	0
#11	0.003	0
#12	0.026	0
#13	0.017	0.017
#14	0	0

3020.1 to 2559.0, a significant reduction of about 15.3%. Travel time is also less. However, while the total cost decreases from $3020.1 to $2,610.30, the operational cost of the gas network is about 7% higher due to energy hub unit consumption. Under normal conditions, all loads are satisfied, so the penalty cost is zero for cases #3 and #4.

Tables 6 and 7 illustrate the traffic flow for the OD pairs' candidate routes during the operational horizon; for example, the first OD pair travels from the High-Level Bridge to the Art Gallery of Alberta; the route comprised of 97th Ave., Bellamy Hill Rd., Jasper Ave., and 100th St. is the fastest and, therefore, the first candidate route.

During peak traffic hours, candidate routes #2 and #3 for the first OD pair are viable. Drivers can use route #3 during hours 14-19 to have optimal travel after the first route reaches its full capacity. During hours 16-18, routes #1 and #3 reach capacity, so drivers should take route #2.

C. ASSESSMENT OF OUTAGES AND OPTIMAL LOCATIONS FOR LOAD SHEDDING

This section demonstrates the effects of distributed generator outages and roadway closures due to maintenance or unusual events. It posits the tripping of the distributed generator located at bus #5 and the closure of road #15. Table 8 presents the operational cost of the PGT network for case studies #3 and #4, representing Edmonton's independent and proposed integrated networks, respectively. Notably, power system and traffic network contingencies do not influence the natural gas system in independent operation mode (case study #3), resulting in a constant operation cost.

Distributed generators play a significant role in supplying local consumers in understudied urban areas. In the distributed generator tripping condition, operators maintain power system operation within a secure range through load shedding. The gas network actively participates in integrated power supply via energy hubs under both contingency and non-contingency conditions, which reduces overall PGT network operational cost. For instance, in independent mode, the penalty cost of load shedding for the distributed generator trip contingency is $18,724.00 but only $9,817.05 for the proposed integrated PGT network, lowering total operational cost from $25,768.02 to $16,460.29. Specifically, the power system's cost in the integrated PGT network decreases from $5,220.00 to $3,377.54, while the gas network cost increases from $1,279.80 to $2,996.35. The travel cost to the traffic system increases approximately 50% due to load curtailment in some power system buses connected to charging stations. Table 9 lists optimal locations for load shedding. In independent mode, load shedding occurs in power system buses #4, #5, and #12, where some charging stations are connected. Although load curtailments are not extensive in scale, they are expensive and affect the operational conditions of other infrastructures. Furthermore, the detailed analysis of Table 9 shows that the integrated PGT network limits load-shedding to buses #2 and #13 during a generator trip, in contrast to the broader impact observed in the independent system. This pinpointing of optimal load-shedding locations underscores the integrated operation policy's effectiveness in reducing the extent of load-shedding required, thus significantly lowering the total operational costs from $25,768.02 to $16,460.29. This evidence of enhanced system resilience and cost-efficiency underlines the practical benefits of the proposed integrated operational policy during component outages.

The closure of road #15 due to maintenance or city events alters optimal travel plans, charging patterns, power flows, and traffic flows. Table 8 shows that the travel cost for the independent system is approximately 9.4%

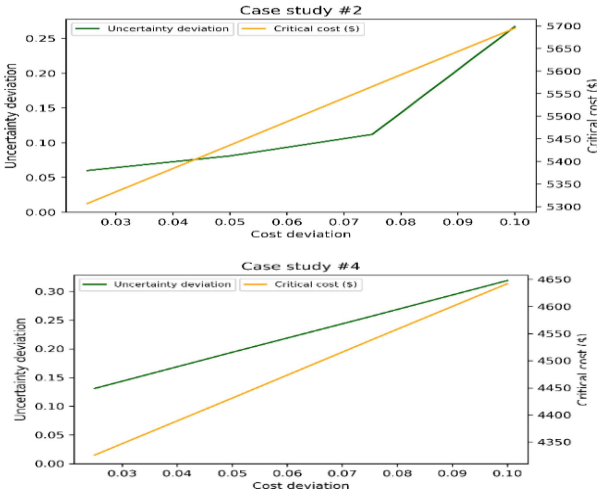

FIGURE 7. Case Studies #2 and #4: Optimal risk-averse uncertainty deviation versus guaranteed cost.

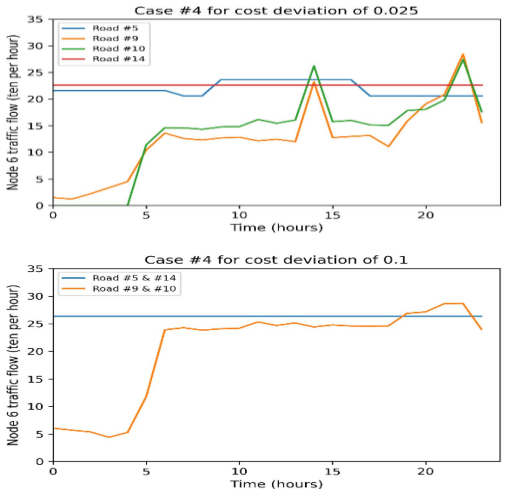

FIGURE 8. Optimal traffic flows on Edmonton roads #5, #9, #10, and #14 for the cost deviations of 0.025 and 0.1.

higher than that for the integrated PGT network. The power system's operational cost decreases from $3,470.10 to $2,998.47, while the gas network's participation increases its cost by about 10.3% over that of the independent mode. Overall, the total operational cost of Edmonton's integrated PGT network is approximately 6.97% less because the gas network provides better options for users when road #15 is closed.

D. IGR STRATEGY FOR THE INTEGRATED PGT NETWORK

For solving the IGR-based problem, the proposed algorithm must include the expected total cost as an input to set the interval of critical cost. This deterministic problem is solved based on the forecast values of the uncertain parameters. Optimal, risk-averse function and guaranteed cost can then be obtained by implementing the IGR strategy on the proposed solar-based PGT model. Figure 7 shows the optimal deviations of the uncertain parameters versus the critical cost for different values of the cost-deviation factor (e.g., from 0 to 0.1) for Case Studies #2 and #4. In Case #4, for cost deviations of 0.025 and 0.075, respectively, if the uncertainty error μ is less than 0.131 and 0.256, critical costs of $4,326 and $4,537 can be guaranteed. In other words, to achieve a cost increase of 7.5%, actual traffic demand must not exceed the forecast demand by 125.6%. Likewise, in Case #2, a cost of $5,436 can be guaranteed if all the uncertain deviations are less than 8.1%. The charging stations' electricity consumption for the scheduling horizon is affected by critical conditions that increase traffic demand. For instance, Figure 8 denotes traffic flows on roads #5, #9, #10, and #14, which lead to the node 6 charging station (bus #14 power network), as $\rho = 0.025$ and 0.1. Since demand is greater when $\rho = 0.1$, most of the traffic flows on $\rho = 0.1$ roads are heavier than those on $\rho = 0.025$ roads. For example, from hours 1 to 5, the flow on road #10, Jasper Avenue, between the intersections with 101st and 102nd Streets, when $\rho = 0.025$, is 0 and increases to about 60 vehicles per hour, when $\rho = 0.1$. When traffic demands become critical, flows on roads #5 and #14 and on #9 and #10 are equal. In other words, drivers on road #5 continued their route through road #14 and road #9 drivers continued on road #10.

E. PERFORMANCE EVALUATION OF THE PROPOSED PGT MODEL BASED ON AFTER-THE-FACT ANALYSIS

Deterministic and scenario-based stochastic algorithms based on forecast values, generated using a 1DCNN-BLSTM algorithm, were used to address the PGT network operation problem and assess the utility and effectiveness of the proposed IGR method. Note that the stochastic optimization approach models various uncertain parameters, while the deterministic optimization problem does not consider uncertainties or prediction errors. Thus, the objective of the problem is calculated based on these optimized variables and the actual values of traffic flow for the day of an event, providing an after-the-fact analysis. Table 10 presents the calculated total costs of the proposed PGT model for the deterministic, stochastic, and IGR methods, considering the actual traffic flow and optimal PGT settings. In addition, Case Study #4 examines both the forecast and actual traffic flows for an arbitrary week in Edmonton. Figure 9 shows the actual [31] and forecast values for this sample week; note that over the last four days, most traffic flows were underestimated. These results confirm that the total cost of the risk-averse IGR method is lower than the other algorithms. When underestimation is likely, the proposed method operates economically.

F. EVALUATION OF THE PROPOSED FRAMEWORK FOR A 24-NODE TRAFFIC NETWORK

This subsection evaluates the effectiveness of the proposed PGT network through a 24-node, 37-road traffic network, incorporating eleven OD pairs and five fast charging stations,

TABLE 10. After-the-fact analysis of the case study #4.

Days	Scenario-based stochastic cost ($)	Deterministic cost ($)	Risk-averse IGR cost ($) for ρ =0.025
#1	4590.0	4562.8	4601.7
#2	4556.2	4560.5	4563.3
#3	4499.1	4420.7	4330.2
#4	4564.5	4496.4	4456.7
#5	4508.2	4500.1	4423.9
#6	4583.9	4479.0	4401.4
#7	4516.0	4431.7	4389.1
Weekly total cost	31817.9	31451.2	31166.3

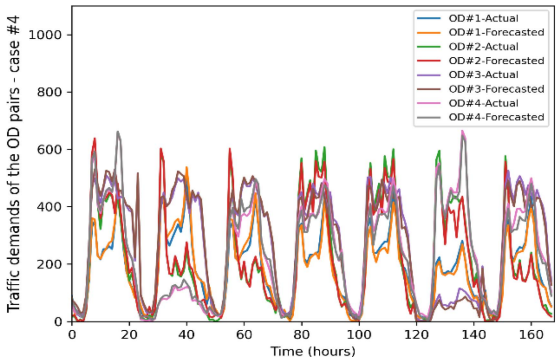

FIGURE 9. Traffic demand values for a sample week.

TABLE 11. Characteristics of the 24-node traffic network.

Locations of the OD pairs			Locations of the EV charging stations	
OD pairs	Origin (traffic network's node)	Destination (traffic network's node)	Location on the Traffic network (#node)	Location on the electrical network (#bus)
#1	#1	#13	#7	#4
#2	#9	#15		
#3	#3	#12		
#4	#4	#16	#10	#5
#5	#6	#14		
#6	#8	#22	#12	#8
#7	#9	#12		
#8	#18	#14	#16	#12
#9	#17	#24		
#10	#10	#5	#22	#14
#11	#19	#23		

TABLE 12. Traffic flow demands of the 24-node traffic network's OD pairs.

Time (Hour)	#OD pairs										
	#1	#2	#3	#4	#5	#6	#7	#8	#9	#10	#11
#1	50	40	80	10	40	20	10	70	20	50	10
#2	60	30	80	10	40	20	30	70	20	50	10
#3	60	40	60	10	50	30	30	70	20	60	10
#4	70	40	60	20	60	40	30	70	40	60	10
#5	170	40	110	20	70	50	30	80	40	60	10
#6	400	140	340	50	110	80	50	110	70	230	40
#7	510	150	370	160	320	220	70	350	70	330	160
#8	580	150	370	150	340	220	180	380	290	420	190
#9	300	100	180	130	310	200	140	430	260	410	130
#10	250	90	180	140	190	90	140	230	170	290	90
#11	280	90	80	40	100	90	90	240	110	300	80
#12	250	100	250	100	150	150	100	240	120	300	80
#13	450	110	230	120	120	150	90	300	200	310	110
#14	480	110	200	150	160	170	110	310	220	300	120
#15	480	120	210	150	150	180	110	320	220	300	120
#16	600	200	450	210	400	350	220	450	300	500	240
#17	610	200	450	210	400	300	220	430	320	550	240
#18	610	220	450	200	400	300	200	430	350	550	250
#19	500	190	300	150	300	240	160	370	200	380	160
#20	460	100	240	100	220	160	110	310	120	220	100
#21	270	90	170	70	190	130	80	240	50	100	50
#22	150	70	130	60	130	100	50	160	30	50	40
#23	90	50	100	30	60	40	20	90	20	50	20
#24	50	40	90	10	50	40	20	70	20	60	20

TABLE 13. Optimal operational results of 24-node traffic model integrated PGT network.

Operation Policy	Total cost ($)	Electrical Network cost ($)	Gas Network cost ($)	Travel Cost ($)	Emission (lb)
Independent	7051.2	4161.3	2038.2	851.5	4213.0
Integrated	6743.8	3649.1	2419.7	674.9	3509.4

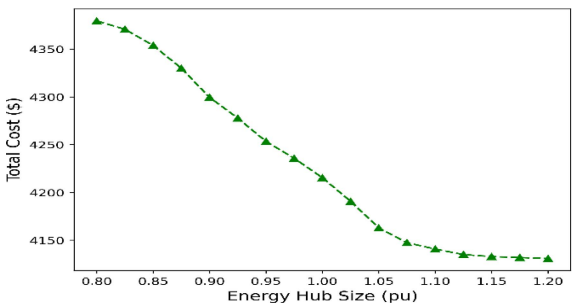

FIGURE 10. Sensitivity analysis for PGT total cost based on different energy hub sizes.

each equipped with seven units. The origins, destinations, and charging station locations are detailed in Table 11. Table 12 illustrates the traffic demands for OD pairs in the presented 24-node traffic network, with each OD pair featuring three candidate routes. The analysis presented in Table 13 compares operational costs and emission impacts under independent and integrated operational policies. The integrated policy achieves a 16.7% reduction in greenhouse gas emissions, highlighting its environmental advantage. As previously noted, the gas network's integration is pivotal for meeting the power system's demands, resulting in a 15% increase in gas system operational costs, whereas electrical network costs decrease from $4161.3 to $3649.1. Travel costs also see a reduction of about 20.7%. Consequently, the total cost associated with the integrated PGT network is up to 4.3% lower than that under the independent policy, demonstrating the model's enhanced cost-effectiveness and applicability for large-scale integrated networks.

G. SENSITIVITY ANALYSIS FOR PGT TOTAL COST

This subsection evaluates the impact of varying energy hub sizes, a critical parameter in the proposed PGT network model, on the total cost. By exploring energy hub sizes from 0.8 pu to 1.2 pu, the analysis presented in Fig. 10 demonstrates a clear relationship between hub size and network cost efficiency. Notably, the results indicate a significant decrease in total cost with an increase in energy hub size up to 1.15 pu, after which further increases do not yield substantial cost benefits. This pivotal result not only pinpoints 1.15 pu as the optimal capacity for energy hubs, thereby significantly enhancing cost efficiency in the PGT network, but also underscores the model's robustness and

practicality by demonstrating its responsiveness to variations in essential parameters.

V. CONCLUSION

This paper proposes an approach to optimize routing and energy management of an urban, integrated, renewable-based PGT network. Its effectiveness was tested on the network in Edmonton, a Canadian leader in developing EV fast charging stations. The applied IGR algorithm gives decision-makers the flexibility to handle undesirable uncertain conditions optimally. In addition, it guarantees the total cost for worst cases related to the uncertain parameters. EV users can select routes that minimize travel time and optimize charging strategy, while CFV drivers can choose the least costly routes.

Integrating the gas network with the PT network has broader efficiencies. Leveraging this approach can significantly reduce the undesirable gas emissions of conventional fossil fuel-powered generation systems. It reduces the total operational cost of Edmonton's integrated PGT network during events like the closure of road #15 by approximately 6.97%. The results guarantee a total cost 7.5% higher than the expected cost if traffic demand does not exceed 125.6% of the forecast value. Using the proposed method to modify EV charging patterns optimized travel time and significantly reduced the operational costs of the PGT network. Based on simulation results, the total cost of Edmonton's integrated PGT network is approximately 5.4% less than that under the independent mode of operation.

REFERENCES

[1] S. F. Batista, M. Ameli, and M. Menéndez, "On the characterization of eco-friendly paths for regional networks," *IEEE Open J. Intell. Transp. Syst.*, vol. 4, pp. 204–215, 2023.

[2] "Electric vehicles." Accessed: Dec. 1, 2022. [Online]. Available: https://www.edmonton.ca/city_government/environmental_stewardship/electric-vehicles

[3] "Downtown district energy system project." Accessed: Dec. 1, 2022. [Online]. Available: https://www.epcor.com/products-services/infrastructure/construction-projects/Documents/downtown-district-energy-project-notice.pdf

[4] C. Yao, S. Chen, and Z. Yang, "Joint routing and charging problem of multiple electric vehicles: A fast optimization algorithm," *IEEE Trans. Intell. Transp. Syst.*, vol. 23, no. 7, pp. 8184–8193, Jul. 2022.

[5] N. Hohmann, S. Brulin, J. Adamy, and M. Olhofer, "Three-dimensional urban path planning for aerial vehicles regarding many objectives," *IEEE Open J. Intell. Transp. Syst.*, vol. 4, pp. 839–852, 2023.

[6] Y. Cui, Z. Hu, and X. Duan, "Optimal pricing of public electric vehicle charging stations considering operations of coupled transportation and power systems," *IEEE Trans. Smart Grid*, vol. 12, no. 4, pp. 3278–3288, Jul. 2021.

[7] T. Zhao, H. Yan, X. Liu, and Z. Ding, "Congestion-aware dynamic optimal traffic power flow in coupled transportation power systems," *IEEE Trans. Ind. Informat.*, vol. 19, no. 2, pp. 1833–1843, Feb. 2023.

[8] S. Lv, Z. Wei, G. Sun, S. Chen, and H. Zang, "Optimal power and semi-dynamic traffic flow in urban electrified transportation networks," *IEEE Trans. Smart Grid*, vol. 11, no. 3, pp. 1854–1865, May 2020.

[9] R. Dhanasekar, L. Vijayaraja, V. Kanakasri, S. Raadha, and T. Swami, "Future of electric transportation: A qualitative study on how decarbonization can be improved by effective analysis," in *Proc. 6th IEEE Int. Conf. Trends Electron. Informat. (ICOEI)*, Tirunelveli, India, Apr. 2022, pp. 154–162.

[10] F. Wei, X. Zhang, J. Chu, F. Yang, and Z. Yuan, "Energy and environmental efficiency of China's transportation sectors considering CO_2 emission uncertainty," *Transp. Res. Part D: Transp. Environ.*, vol. 97, Jun. 2021, Art. no. 102955.

[11] S. Lv, S. Chen, Z. Wei, and H. Zhang, "Power-transportation coordination: Toward a hybrid economic-emission dispatch model," *IEEE Trans. Power Syst.*, vol. 37, no. 5, pp. 3969–3981, Sep. 2022.

[12] Y. Yu, S. Li, H. Sun, and F. Taghizadeh-Hesary, "Energy carbon emission reduction of China's transportation sector: An input–output approach," *Econ. Anal. Policy.*, vol. 69, pp. 378–393, Mar. 2021.

[13] Y. Yin, C. He, T. Liu, and L. Wu, "Risk-averse stochastic midterm schedule of thermal-hydro-wind system: A network-constrained clustered unit commitment approach," *IEEE Trans. Sustain. Energy*, vol. 13, no. 3, pp. 1293–1304, Jul. 2022.

[14] A. Dolatabadi, H. Abdeltawab, and Y. A.-R. I. Mohamed, "A novel model-free deep reinforcement learning framework for energy management of a PV integrated energy hub," *IEEE Trans. Power Syst.*, vol. 38, no. 35, pp. 4840–4852, Sep. 2023.

[15] H. Mousavi-Sarabi, M. Jadidbonab, and B. Mohammadi Ivatloo, "Stochastic assessment of the renewable–based multiple energy system in the presence of thermal energy market and demand response program," *J. Operat. Autom. Power Eng.*, vol. 8, pp. 22–31, Feb. 2020.

[16] M. Jadidbonab, B. Mohammadi-Ivatloo, M. Marzband, and P. Siano, "Short-term self-scheduling of virtual energy hub plant within thermal energy market," *IEEE Trans. Ind. Electron.*, vol. 68, no. 4, pp. 3124–3136, Apr. 2021.

[17] A. Ebrahimi-Moghadam and M. Farzaneh-Gord, "Optimal operation of a multi-generation district energy hub based on electrical, heating, and cooling demands and hydrogen production," *Appl. Energy*, vol. 309, Mar. 2022, Art. no. 118453.

[18] M. Jadidbonab, E. Babaei, and B. Mohammadi-ivatloo, "CVaR-constrained scheduling strategy for smart multi carrier energy hub considering demand response and compressed air energy storage," *Energy*, vol. 174, pp. 1238–1250, May 2019.

[19] S. Paul, A. Sharma, and N. P. Padhy, "Risk constrained energy efficient optimal operation of a converter governed AC/DC hybrid distribution network with distributed energy resources and volt-VAR controlling devices," *IEEE Trans. Ind. Appl.*, vol. 57, no. 4, pp. 4263–4277, Jul./Aug. 2021.

[20] M. Daneshvar, B. Mohammadi-Ivatloo, and K. Zare. "A fair risk-averse stochastic transactive energy model for 1% renewable multi-microgrids in the modern power and gas incorporated network," *IEEE Trans. Smart Grid*, vol. 14, no. 3, pp. 1933–1945, May 2023.

[21] A. Dolatabadi, M. Jadidbonab, and B. Mohammadi-ivatloo, "Short-term scheduling strategy for wind-based energy hub: A hybrid stochastic/IGDT approach," *IEEE Trans. Sustain. Energy*, vol. 10, no. 1, pp. 438–448, Jan. 2019.

[22] M. Jadidbonab, S. Madadi, and B. Mohammadi-ivatloo, "Hybrid strategy for optimal scheduling of renewable integrated energy hub based on stochastic/robust approach," *J. Energy Manag. Technol.*, vol. 2, no. 4, pp. 29–38, Nov. 2018.

[23] W. Wei, L. Wu, J. Wang, and S. Mei, "Expansion planning of urban electrified transportation networks: A mixed-integer convex programming approach," *IEEE Trans. Transport. Electrific.*, vol. 3, no. 1, pp. 210–224, Mar. 2017.

[24] C. D. Vasconcelos, S. R. Lourenço, A. C. Gracias, and D. A. Cassiano, "Network flows modeling applied to the natural gas pipeline in Brazil," *J. Nat. Gas sci. Eng.*, vol. 14, pp. 211–224, Sep. 2013.

[25] A. Shabanpour-Haghighi, and A. R. Seifi, "An integrated steady-state operation assessment of electrical, natural gas, and district heating networks," *IEEE Trans. Power Syst.*, vol. 31, no. 5, pp. 3636–3647, Sep. 2016.

[26] A. Martinez-Mares, and C. R. Fuerte-Esquivel, "A unified gas and power flow analysis in natural gas and electricity coupled networks," *IEEE Trans. Power Syst.*, vol. 27, no. 4, pp. 2156–2166, Nov. 2012.

[27] "Geo model solar Co." Accessed: Dec. 1, 2022. [Online]. Available: https://solargis.info/imaps/

[28] M. Jadidbonab, A. Dolatabadi, B. Mohammadi-Ivatloo, M. Abapour, and S. Asadi, "Risk-constrained energy management of PV integrated smart energy hub in the presence of demand response program and compressed air energy storage," *IET Renew. Power Generat.*, vol. 13, no. 6, pp. 998–1008, Apr. 2019.

[29] "Alberta energy profile." Accessed: Dec. 1, 2022. [Online]. Available: https://www.cer-rec.gc.ca/en/data-analysis/energy-markets/provincial-territorial-energy-profiles/provincial-territorial-energy-profiles-alberta.html
[30] City of edmonton traffic flow map." Accessed: Dec. 1, 2022. [Online]. Available: https://www.edmonton.ca/sites/default/files/public-files/assets/RoadsTraffic/Flow_map_2015_AAWDT.pdf
[31] "Traffic volumes, Edmonton." Accessed: Dec. 1, 2022. [Online]. Available: https://www.edmonton.ca/transportation/traffic_reports/traffic-volumes-turning-movements
[32] Public charging stations." Accessed: Dec. 1, 2022. [Online]. Available: https://data.edmonton.ca/Environmental-Services/Public-Charging-Stations-for-Electric-Vehicles-Map/rg5m-e4tk
[33] T. Niknam, A. Kavousifard, S. Tabatabaei, and J. Aghaei, "Optimal operation management of fuel cell/wind/photovoltaic power sources connected to distribution networks," *J. Power Sour.*, vol. 196, no. 20, pp. 8881–8896, Oct. 2011.
[34] W. Gan et al., "Coordinated planning of transportation and electric power networks with the proliferation of electric vehicles," *IEEE Trans. Smart Grid*, vol. 11, no. 5, pp. 4005–4016, Sep. 2020.

MOHAMMAD JADIDBONAB (Graduate Student Member, IEEE) was born in Tabriz, Iran, in 1992. He received the B.Sc. and M.Sc. degrees in electrical engineering from the University of Tabriz, Tabriz, in 2015 and 2017, respectively. He is currently pursuing the Ph.D. degree with the University of Alberta, Edmonton, AB, Canada. From 2017 to 2020, he was a Research Assistant with the Smart Energy Systems Laboratory, University of Tabriz. His research interests include the application of artificial intelligence, machine learning, deep learning, and data analytics to multicarrier energy systems.

HUSSEIN ABDELTAWAB (Senior Member, IEEE) was born in Bani-Souwaif, Egypt, in April 1987. He received the B.Sc. (with Hons.) and M.Sc. degrees in electrical engineering from Cairo University in 2009 and 2012, respectively, and the Ph.D. degree in electrical engineering from the University of Alberta, Edmonton, AB, Canada, in 2017.

He is currently an Assistant Professor of Engineering with Wake Forest University, Winston-Salem, NC, USA. He is also a licensed Professional Engineer in Saskatchewan, Canada. His research interests include energy management, machine learning applications in renewable energy, energy storage, and smart distribution systems. He is the Chair of the IEEE Winston-Salem Section. He is also an Associate Editor of the *IET Generation, Transmission, and Distribution*.

YASSER ABDEL-RADY I. MOHAMED (Fellow, IEEE) was born in Cairo, Egypt, in November 1977. He received the B.Sc. (Hons.) and M.Sc. degrees in electrical engineering from Ain Shams University, Cairo, in 2000 and 2004, respectively, and the Ph.D. degree in electrical engineering from the University of Waterloo, Waterloo, ON, Canada, in 2008. He is a Professor with the Department of Electrical and Computer Engineering, University of Alberta, Edmonton, AB, Canada. His highly cited research focuses on modeling, analysis, stability, control, and optimization of power electronic converters and systems, active distribution systems, and microgrids; grid integration of distributed and renewable energy resources and energy storage; and the development of artificial intelligence technologies for smart grids. He is an Associate Editor of the IEEE TRANSACTIONS ON POWER ELECTRONICS. He was an Editor of the IEEE TRANSACTIONS ON POWER SYSTEMS, IEEE TRANSACTIONS ON SMART GRID, and IEEE POWER ENGINEERING LETTERS, and an Associate Editor of the IEEE TRANSACTIONS ON INDUSTRIAL ELECTRONICS. He is an Elected Fellow of the Asia-Pacific Artificial Intelligence Association. He is a registered Professional Engineer in the Province of Alberta, Canada.